The Astrophysical Journal, 739:1 (13pp), 2011 September 20 doi:10.1088/0004-637X/739/1/1

EXPLORING THE GALAXY MASS–METALLICITY RELATION AT $z \sim 3$–5

Tanmoy Laskar[1], Edo Berger[1], and Ranga-Ram Chary[2]
[1] Harvard-Smithsonian Center for Astrophysics, 60 Garden Street, Cambridge, MA 02138, USA
[2] Spitzer Science Center, California Institute of Technology, Pasadena, CA 91125, USA
Received 2011 February 4; accepted 2011 June 15; published 2011 August 26

ABSTRACT

Long-duration gamma-ray bursts (GRBs) provide a premier tool for studying high-redshift star-forming galaxies thanks to their extreme brightness and association with massive stars. Here we use GRBs to study the galaxy stellar mass–metallicity (M_*–Z) relation at $z \sim 3$–5, where conventional direct metallicity measurements are extremely challenging. We use the interstellar medium metallicities of long GRB hosts derived from afterglow absorption spectroscopy, in conjunction with host galaxy stellar masses determined from deep *Spitzer* 3.6 μm observations of 20 GRB hosts. We detect about 1/4 of the hosts with $M_{\rm AB}(I) \approx -21.5$ to -22.5 mag and place a limit of $M_{\rm AB}(I) \gtrsim -19$ mag on the remaining hosts from a stacking analysis. Using these observations, we present the first rest-frame optical luminosity distribution of long GRB hosts at $z \gtrsim 3$ and find that it is similar to the distribution of long GRB hosts at $z \sim 1$. In comparison to Lyman-break galaxies at the same redshift, GRB hosts are generally fainter, but the sample is too small to rule out an overall similar luminosity function. On the other hand, the GRB hosts appear to be more luminous than the population of Lyα emitters at $z \sim 3$–4. Using a conservative range of mass-to-light ratios for simple stellar populations (with ages of 70 Myr to $\sim$2 Gyr), we infer the host stellar masses and present mass–metallicity measurements at $z \sim 3$–5 ($\langle z \rangle \approx 3.5$). We find that the detected GRB hosts, with $M_* \approx 2 \times 10^{10}\ M_\odot$, display a wide range of metallicities, but that the mean metallicity at this mass scale, $Z \approx 0.3\ Z_\odot$, is lower than measurements at $z \lesssim 3$. Combined with stacking of the non-detected hosts with $M_* \lesssim 3 \times 10^9\ M_\odot$ and $Z \lesssim 0.1\ Z_\odot$, we find tentative evidence for the existence of an M_*–Z relation at $z \sim 3.5$ and continued evolution of this relation to systematically lower metallicities from $z \sim 2$.

Key words: galaxies: high-redshift – galaxies: ISM – galaxies: luminosity function, mass function – gamma-ray burst: general – infrared: galaxies

Online-only material: color figures

1. INTRODUCTION

The simple "closed-box" model of galaxy evolution (Talbot & Arnett 1971) predicts a correlation between the stellar mass and the gas-phase metallicity of a galaxy (the M_*–Z relation), under the assumptions of no gas inflows or outflows, a constant yield of metals, an invariant stellar initial mass function (IMF), and instantaneous mixing of newly synthesized metals back into the interstellar medium (ISM). In reality, this simple picture is complicated by the fact that galaxies accrete low-metallicity gas from the intergalactic medium and lose metal-enriched gas through galactic-scale winds or by depletion onto dust. In addition to these processes, the M_*–Z relation may also be modified by a mass-dependent star formation efficiency (Juneau et al. 2005; Feulner et al. 2005; Franceschini et al. 2006; Asari et al. 2007), and possibly an environmental-dependent IMF (Köppen et al. 2007). Thus, the M_*–Z relation and its evolution with redshift provide insight into the physical processes that shape galaxy formation and evolution across cosmic time.

Given the importance of this relation it has been the focus of several extensive studies out to $z \sim 3$. In the local universe ($z \sim 0.1$), Tremonti et al. (2004) studied 53,400 galaxies from the Sloan Digital Sky Survey (SDSS) and found a tight correlation ($\pm$0.1 dex) between stellar mass and metallicity over a range of $M_* \approx 10^{8.5}$–$10^{11.5}\ M_\odot$ and an order of magnitude in metallicity (see also Kewley & Ellison 2008). They concluded that the observed correlation is best explained by the influence of metal-enriched outflows, with larger metal loss in lower mass galaxies. Studies at $z \sim 1$–3 (Savaglio et al. 2005; Erb et al. 2006; Maiolino et al. 2008; Mannucci et al. 2009; Zahid et al. 2011; Finkelstein et al. 2011) found that the M_*–Z relation evolves by about 0.8 dex from $z \sim 3$ to the present, while keeping the same overall trend. Savaglio et al. (2005) argued that the redshift evolution to $z \sim 0.7$ can be reproduced in the simple closed-box model with the assumption that the typical timescale for star formation is longer in lower mass galaxies. On the other hand, Zahid et al. (2011) found that the M_*–Z relation evolves only below $\sim 10^{10.5}\ M_\odot$ to $z \sim 0.8$, and argued that unlike in the local universe the effective yield decreases with larger mass and that a closed-box model cannot explain the evolution. They further argued that outflows play a minor role and proposed that a rising star formation efficiency with large mass may be the dominant effect. Erb et al. (2006) argued that at $z \sim 2.3$ the primary driving mechanism for the M_*–Z relation and its evolution is the expected increase in metallicity as star formation leads to a reduced gas fraction, and that outflows affect galaxies at all mass scales.

Beyond $z \sim 2.3$ there are only a few measurements of galaxy metallicities and masses. Mannucci et al. (2009) studied 10 Lyman-break galaxies (LBGs) at $z \sim 3.1$ and found continued downward evolution of the M_*–Z relation and a decreasing effective yield with larger stellar mass. They argued that gas infall plays the dominant role in the M_*–Z relation and that outflows are not needed. Maiolino et al. (2008) studied nine LBGs at $z \sim 3.5$ and found a decline in the mean metallicity at a stellar mass scale of $\sim 1.4 \times 10^{10}\ M_\odot$ compared to $z \sim 2.3$, with a possible steepening of the M_*–Z relation relative to lower redshifts.

Tracing the M_*–Z relation and its evolution to even earlier times will provide insight into the earliest epochs of galaxy

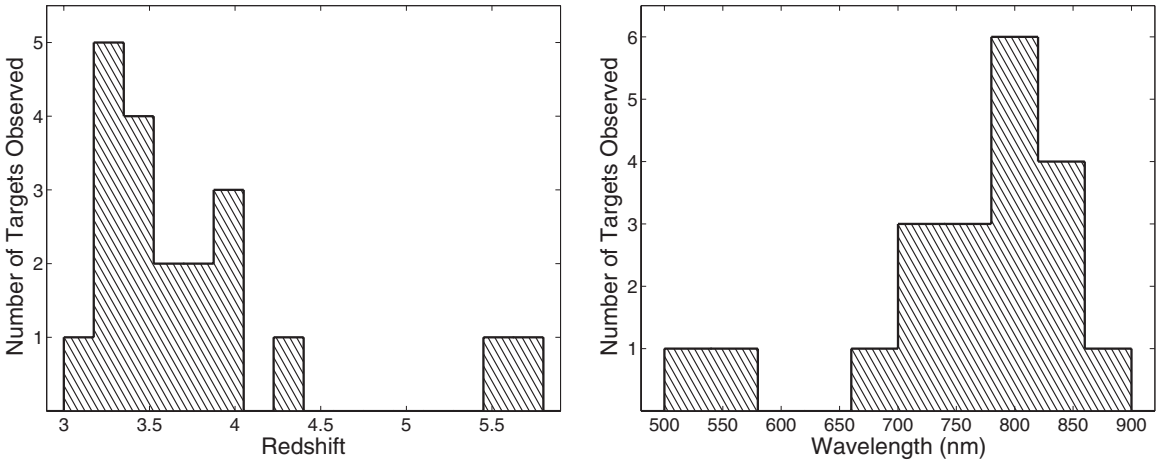

Figure 1. Redshift distribution (left panel) and rest-frame wavelength probed with our *Spitzer*/IRAC 3.6 μm observations (right panel) for the targets in this paper. All observations fall redward of 4000 Å and therefore probe the rest-frame optical.

evolution, while allowing us to probe the relative importance of the various galactic-scale phenomena proposed at $z \lesssim 3$. Although initial studies of LBGs at $z \sim 3.5$ are now available (Maiolino et al. 2008; Mannucci et al. 2009), these studies are challenging because the nebular emission lines required for robust metallicity measurements[3] (e.g., Hα, Hβ, N II λ6583, O III $\lambda\lambda$4959, 5007, and O II $\lambda\lambda$3726, 3729) shift into the near- and mid-IR, where existing spectrographs have reduced sensitivity compared to the optical band. This is further complicated by the rapid dimming of galaxies at higher redshift such that only the most luminous LBGs are amenable to spectroscopy.

An alternative way to determine metallicities at $z \gtrsim 3$ (and in principle at $z \sim 10$ and beyond; Salvaterra et al. 2009; Tanvir et al. 2009) is absorption spectroscopy of gamma-ray burst (GRB) optical/near-IR afterglows. Long-duration GRBs are known to be associated with the deaths of massive stars (e.g., Woosley & Bloom 2006), and therefore with sites of active star formation. The large optical luminosities of GRB afterglows (easily exceeding 20 mag for several hours even at $z \sim 8$; Tanvir et al. 2009), and their intrinsic featureless spectra, provide a unique way to measure ISM metallicities for galaxies at $z \gtrsim 2$ from rest-frame ultraviolet metal absorption lines and Lyα absorption. Since the afterglows are significantly brighter than the underlying host galaxies, this technique allows us to measure metallicities independent of the galaxy brightness. Moreover, since long GRB progenitors reside in star-forming environment within their hosts, their sight lines probe the warm ISM and H II regions that give rise to the (rest-frame optical) nebular emission lines that are used for metallicity measurements at $z \lesssim 3$. This approach has now been exploited at least to $z \sim 5$ using optical spectra (e.g., Berger et al. 2006; Prochaska et al. 2007; Fynbo et al. 2009), and with near-IR spectrographs it can be implemented to $z \sim 20$.

Naturally, to explore the M_*–Z relation at $z \gtrsim 3$ we also require a determination of the GRB host galaxy stellar masses, and hence follow-up infrared observations with the *Spitzer Space Telescope* to probe the rest-frame optical luminosity. Here, we present the first large set of *Spitzer* observations for GRB host galaxies at $z \sim 3$–5 and combine the inferred masses with measured metallicities to explore the M_*–Z relation beyond $z \sim 3$. Since deep *Spitzer*/Infra-Red Array Camera (IRAC) images are generally confusion-limited, our use of GRB afterglows provides an additional boon—they accurately pinpoint the location of the host galaxies (to $\sim$0.″1), thereby allowing for accurate galaxy identifications.[4] The plan of the paper is as follows. We present the *Spitzer* observations, analysis, photometry, and metallicity data in Section 2. In Section 3.1, we present the first rest-frame optical luminosity distribution of GRB hosts at $z \gtrsim 3$ and compare it to both $z \sim 1$ GRB hosts and field galaxy samples at $z \sim 3$. We derive the mass distribution in Section 3.2. Finally, in Section 4 we combine the mass and metallicity measurements to place the first points on the M_*–Z diagram at $z \gtrsim 3$. We explore the implications of our results and future prospects in Section 5.

2. GRB SAMPLE AND DATA ANALYSIS

We obtained deep observations of all 35 long GRB host galaxies with spectroscopic redshifts in the range $z \approx 2$–5.8 available as of 2006 November using the 3.6 μm band of the IRAC (Fazio et al. 2004) on board the *Spitzer Space Telescope*. Here we investigate the properties of GRB hosts in the redshift range $z \approx 3$–5.6 (observed for about 2 hr each); targets at redshifts $z \approx 2$–3 are treated elsewhere (R.-R. Chary et al. 2011, in preparation). For the objects in this paper, the effective wavelength of the IRAC 3.6 μm band probes the rest-frame spectral energy distribution (SED) redward of about 5500 Å (Figure 1) and therefore provides a robust measure of the stellar mass (Section 3.2).

We processed the *Spitzer* data using the standard MOPEX (Makovoz et al. 2006) software package to generate mosaics for each target. The MOPEX package detects and removes cosmic rays and moving objects before drizzling (Fruchter & Hook 2002), performing background equalization, and applying distortion corrections. For our coverage and dither pattern we find that an output pixel scale of 0.″4 and a drizzling parameter of

[3] For example, Mannucci et al. (2009) use the R_{23} diagnostic to determine metallicities for their $z \sim 3$ galaxy sample, but this relation is known to be double-valued. They attempt to discriminate between the low- and high-metallicity branches using the O III λ5007/O II λ3727 ratio.

[4] This can be contrasted with the potential use of quasar *intervening* absorption systems for studies of the M_*–Z relation, since the galaxy counterparts of the absorbers are offset on the sky by $\sim$ few arcseconds from the quasar position. Spectroscopic confirmation is therefore required to determine the correct counterpart, rendering the advantage of absorption spectroscopy void. Furthermore, even if the galaxy counterparts could be identified, observations with *Spitzer*'s large point-spread function against the much brighter quasar glare are essentially impossible.

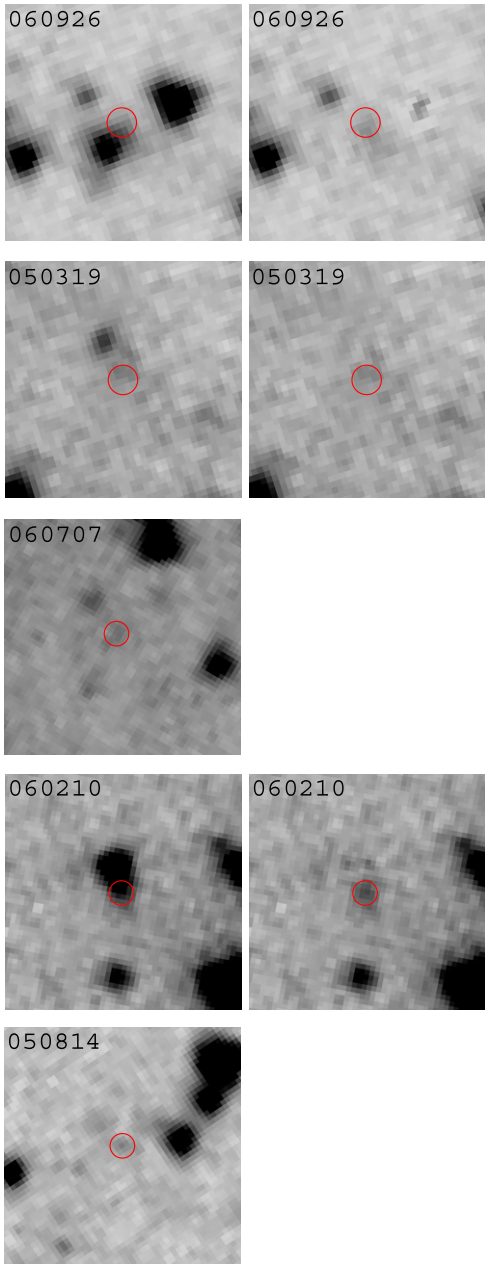

Figure 2. *Spitzer* images of the GRB host galaxies with 3.6 μm detections. The left-hand panels show the processed images, while the right-hand panels include subtractions of nearby sources using GALFIT (when performed). The circles (1″ radius) mark the afterglow positions. All images have the same orientation (north is up and east is to the left) and scale (16″ on a side) with 0.″4 square pixels.

(A color version of this figure is available in the online journal.)

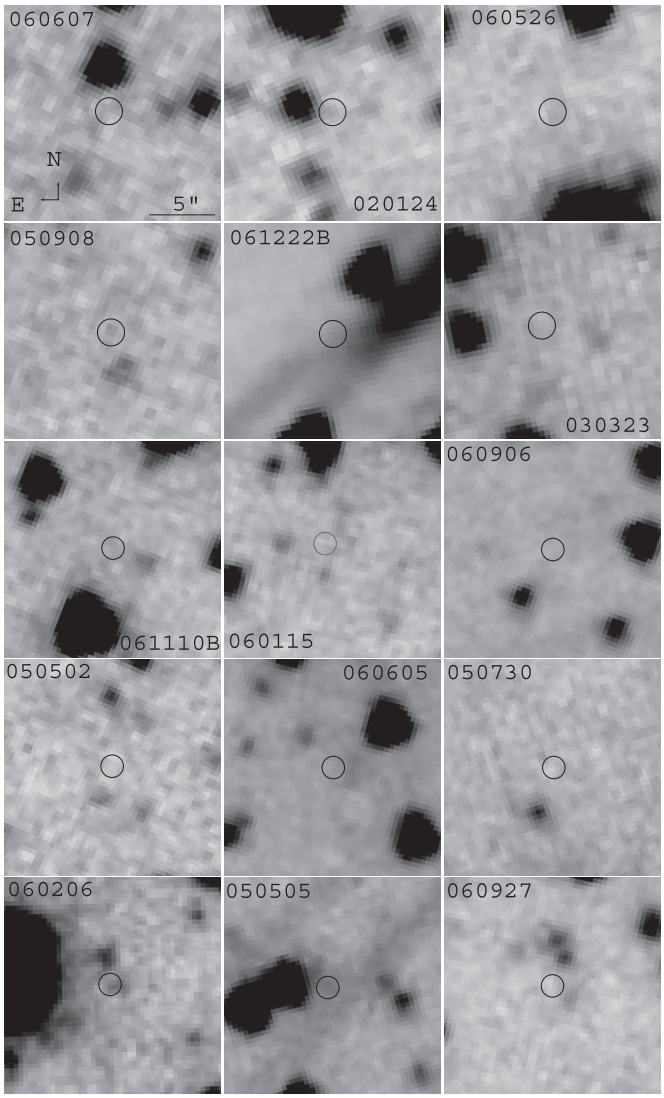

Figure 3. *Spitzer* images of regions around the GRB hosts with 3.6 μm non-detections. The circles (1″ radius) mark the afterglow positions. All images have the same orientation (north is up and east is to the left) and scale (16″ on a side) with 0.″4 square pixels.

0.7 provide the best combination of improvement in the point-spread function (PSF) with minimal degradation of the signal-to-noise ratio. We set all other parameters in MOPEX to their recommended defaults.

2.1. Astrometry

We used optical afterglow images to perform relative astrometry on the *Spitzer* mosaics and to locate the GRB hosts. The median root-mean-square residual of the astrometric ties is about 0.″12, corresponding to about one-tenth of the *Spitzer* PSF at 3.6 μm. This is the dominant source of uncertainty in the astrometry, since the optical afterglow detections themselves are mostly of high signal-to-noise ratio. In only the two cases (GRBs 050502 and 050814) where no afterglow images were available, we performed absolute astrometry based on SDSS and Two Micron All Sky Survey using the afterglow coordinates as reported in the GCN circulars (Jensen et al. 2005; Blake & Bloom 2005). We detect one of these hosts (GRB 050814) in our *Spitzer* follow-up. The *Spitzer* images for the detected hosts are presented in Figure 2, while non-detections are presented in Figure 3.

2.2. Photometry

At the depth of our observations, *Spitzer* images are confusion-limited for faint sources. As a result, in several cases the region around the expected location of the GRB host is contaminated by light from nearby stars or galaxies. Prior to performing photometry, we used the GALFIT software package (Peng et al. 2002) to model and subtract these neighboring sources. For this purpose, we used multiple point sources in each case to determine the mosaic PSF with the IDL STARFINDER routines (Diolaiti et al. 2000). The accuracy of the generated PSF

Table 1
Spitzer Observations and Inferred Properties of GRB Host Galaxies at $z \sim 3$–5 in this Study

GRB	z	$F_\nu(3.6\,\mu\mathrm{m})$ (μJy)	P_{cc}[a]	$M_{AB}(780\,\mathrm{nm})$	$(M/F_\nu)_{70\,\mathrm{Myr}}$ ($10^{10} M_\odot\,\mu\mathrm{Jy}^{-1}$)	$(M/F_\nu)_{\mathrm{max}}$ ($10^{10} M_\odot\,\mu\mathrm{Jy}^{-1}$)	$M_{70\,\mathrm{Myr}}$ ($10^{10}\,M_\odot$)	M_{max} ($10^{10}\,M_\odot$)
020124	3.198	<0.26	...	>−20.29	0.73	3.09	<0.19	<0.80
030323	3.372	<0.21	...	>−20.14	0.79	3.32	<0.17	<0.70
050319	3.240	0.80 ± 0.09	7.7%	−21.53 ± 0.20	0.75	3.14	0.60 ± 0.07	2.51 ± 0.29
050502	3.793	<0.21	...	>−20.32	0.93	3.90	<0.20	<0.82
050730	3.968	<0.26	...	>−20.62	0.99	4.15	<0.26	<1.08
050814	5.77[b]	0.55 ± 0.06	7.6%	−21.94 ± 0.20	1.54	7.75	0.85 ± 0.09	4.26 ± 0.47
050908	3.344	<0.25	...	>−20.31	0.78	3.27	<0.20	<0.82
060115	3.533	<0.31	...	>−20.63	0.85	3.56	<0.26	<1.10
060206	4.048	<0.21	...	>−20.41	1.02	4.29	<0.21	<0.90
060210	3.913	1.41 ± 0.10	5.9%	−22.42 ± 0.11	0.97	4.08	1.37 ± 0.10	5.75 ± 0.41
060526	3.221	<0.25	...	>−20.25	0.74	3.12	<0.19	<0.78
060605	3.773	<0.24	...	>−20.45	0.92	3.88	<0.22	<0.93
060607	3.075	<0.24	...	>−20.14	0.69	2.97	<0.17	<0.71
060707	3.425	1.10 ± 0.10	6.8%	−21.96 ± 0.16	0.81	3.40	0.89 ± 0.08	3.74 ± 0.34
060906	3.686	<0.28	...	>−20.58	0.90	3.76	<0.25	<1.05
060926	3.206	1.65 ± 0.07	4.3%	−22.30 ± 0.07	0.73	3.10	1.21 ± 0.05	5.12 ± 0.22
060927	5.464	<0.21	...	>−20.83	1.44	6.98	<0.30	<1.47
061110B	3.433	<0.25	...	>−20.35	0.82	3.41	<0.20	<0.85

Notes.
[a] Probability of chance coincidence.
[b] This is a photometric redshift (Curran et al. 2008).

was evaluated by fitting and subtracting point sources at various locations on the mosaic. To remove neighboring sources around the expected location of the hosts, we used GALFIT with either point source, Gaussian, or Sersic models as appropriate in order to achieve the lowest level of residuals. In two cases (GRBs 061222B and 050505), the expected location of the host based on the afterglow astrometry fell on the diffraction spike of a saturated star. Since we cannot model the PSF at the required level of accuracy to robustly subtract these diffraction spikes, we do not consider these two sources in the subsequent analysis.

For the remaining 18 targets, we searched within 1.″5 of the afterglow centroid (corresponding to ∼10 kpc at $z \sim 3.5$) and detected five GRB hosts at 3.6 μm (GRBs 050319, 050814, 060707, 060210, and 060926). None of these hosts were detected in the simultaneously observed 5.8 μm IRAC band, which has substantially worse sensitivity. In the two cases (GRBs 060926 and 060210) where a nearby source was subtracted prior to photometry, we found (based on the level of residuals) that the flux we associate with the GRB host cannot be explained by modeling it as part of the subtracted source. For GRB 050908, a visual inspection reveals a coincident flux excess, but photometry indicates that it is consistent with a noise fluctuation. For GRB 060206, the source ∼1.″5 to the west of the afterglow centroid is an unrelated foreground object.

To estimate the probability that one or more of the detected sources are chance superpositions, we ran STARFINDER's source-detection routines on 3.′4 × 3.′4 pixel cutouts of the field around our targets and searched for sources down to 5σ using the PSF generated from the corresponding images. Based on the mean number of sources detected at different thresholds and following Bloom et al. (2002), we assign a false-detection probability given by $P_{cc} = 1 - e^{-\pi R^2 \Sigma(u)}$ to each of our detections (Table 1). Here P_{cc} is the probability of chance coincidence, R is the aperture radius, and $\Sigma(u)$ is the number of sources per unit area down to the flux density u of the detection. The probability that all of our detections are chance coincidences is negligible (10^{-6}), while the probability that none of the targets are chance superpositions is 72%. Thus, whereas it is possible for one or two of our detections to be chance superpositions, it is highly unlikely to be the case for all.

We use the FUNTOOLS package to perform aperture photometry on our detections by placing apertures of two native IRAC pixels (2.″45) in radius and background annuli of 2–6 native pixels (2.″45–7.″34) in radius centered on the detected sources. We choose these values since they allow us to apply standard IRAC aperture corrections,[5] which are relevant for the expected compact sizes of galaxies at $z \gtrsim 3$. In the cases where this choice of radii cause nearby objects above the 3σ level to fall within either the aperture or the background annulus, we mask them out and correct for the lost flux (in both the aperture and annulus) by determining our own aperture correction using mosaics of the IRAC calibration star HD1812095, prepared with identical parameters as for our targets.

We determine uncertainties on our measured flux densities using the uncertainty mosaics created by MOPEX. We carry out aperture photometry in an identical fashion on the (squared) uncertainty images as for the source images themselves, including aperture corrections as described above. In addition, we account for correlated noise due to the drizzling process by incorporating an estimate for it in the flux density uncertainty:[6]

$$\sigma^2_{\mathrm{src}} = A F_{\mathrm{corr}} \left[\sum_{i=1}^{N_A} \sigma^2_{i,A} + \frac{N_A^2}{N_B^2} \sum_{i=1}^{N_B} \sigma^2_{i,B} \right], \quad (1)$$

where σ_{src} is the variance of the source flux density, A is the aperture correction, F_{corr} is the effective number of pixels over which noise is correlated in the mosaic, N_A and N_B are the number of pixels in the aperture and background region, respectively, and $\sigma_{i,A}$ and $\sigma_{i,B}$ are the uncertainty of the flux density in the ith pixel of the aperture and background regions,

[5] See Section 4.10 of the IRAC Instrument Handbook.
[6] See http://wise2.ipac.caltech.edu/staff/fmasci/ApPhotUncert_corr.pdf for a derivation.

Table 2
Spitzer Observations and Inferred Properties of GRB Host Galaxies from Previous Studies

GRB	z	$F_\nu(3.6\,\mu\mathrm{m})$ (μJy)	$M_{\mathrm{AB}}(780\,\mathrm{nm})$ (mag)	$(M/F_\nu)_{70\,\mathrm{Myr}}$ ($10^{10}M_\odot\,\mu\mathrm{Jy}^{-1}$)	$(M/F_\nu)_{\mathrm{max}}$ ($10^{10}M_\odot\,\mu\mathrm{Jy}^{-1}$)	$M_{70\,\mathrm{Myr}}$ ($10^{10}M_\odot$)	M_{max} ($10^{10}M_\odot$)
050904[a]	6.295	<0.27	>-21.29	1.69	9.12	<0.46	<2.46
060223A[b]	4.406	<0.30	>-20.91	1.13	4.89	<0.34	<1.47
060510B[b]	4.942	0.23 ± 0.04	-20.78 ± 0.17	1.29	5.86	0.30 ± 0.05	1.4 ± 0.2
060522[b]	5.110	<0.20	>-20.68	1.34	6.18	<0.27	<1.24
080607[c]	3.036	2.53 ± 0.2	-22.68 ± 0.2	0.67	2.94	1.71 ± 0.15	7.4 ± 0.6

Notes.
[a] Berger et al. (2007).
[b] Chary et al. (2007).
[c] Calculated from Chen et al. (2010), who report $m_{\mathrm{AB}} = 22.9 \pm 0.2$ at 3.6 μm (also see erratum).

respectively. Since our final mosaic has 0.″4 pixels, whereas the native detector pixels are 1.″22 on a side, noise will be correlated over about 3 pixels in our images (the exact correlation function will depend on the drizzling parameter as well, for which we used a value of 0.7). As a conservative estimate, we take F_{corr} to be 3.

The resulting flux densities and upper limits are listed in Table 1. The detections range from about 0.55 to 1.65 μJy, while the typical upper limit is about 0.25 μJy (3σ). We list the *Spitzer* 3.6 μm results for five additional GRB hosts at $z \gtrsim 3$ from the literature (Berger et al. 2007; Chary et al. 2007; Chen et al. 2010) in Table 2.

2.3. Stacking

To assess the typical flux density of the non-detected hosts we carry out a stacking analysis with 11 of the 13 non-detections that have accurate relative astrometry. We exclude GRB 050502, for which we only have absolute astrometry, and GRB 060927, for which the relative astrometry is poor due to a low signal-to-noise detection of the afterglow. The remaining 11 targets are located at a median redshift of $z = 3.4$. We first perform sub-pixel shifts on the *Spitzer* mosaics to bring the expected location of each host (based on the afterglow centroid) to the center of a mosaic pixel using the IRAF task IMSHIFT. We then average 51 × 51 pixel sections from each image centered on the expected location of the host, weighted by the inverse of the corresponding variance maps, after masking out the bright ($>5\sigma$) sources. The resulting stacked image (Figure 4) does not show a detection, and we place a limit of $\lesssim$80 nJy (3σ) on the mean flux density of these 11 hosts.

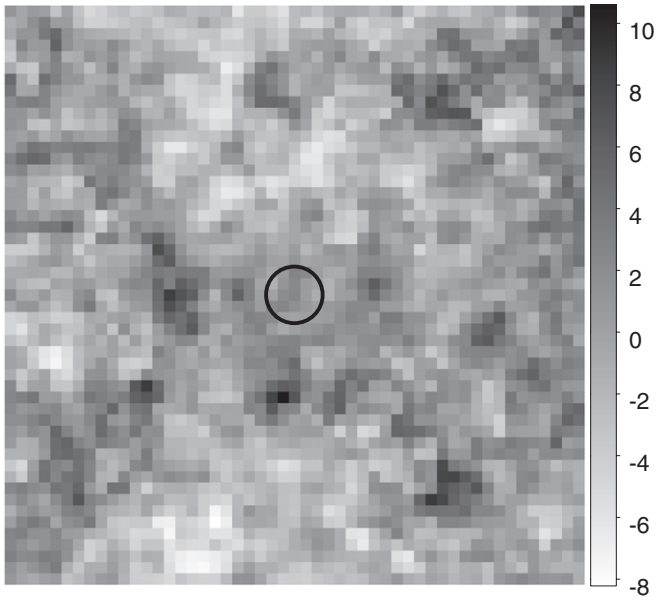

Figure 4. Weighted mean stack of a 51 × 51 pixel region around the location of the 11 GRB hosts with precise astrometry and individual non-detections (image unit nJy/pixel). The circle marks a 1″ radius centered on the expected stack location of the hosts. The non-detection in the stack yields a 3σ upper limit of 80 nJy.

2.4. Metallicities

Absorption spectra of GRB afterglows present a unique opportunity to measure ISM abundances of galaxies at $z \gtrsim 3$, where current spectroscopic sensitivity limits are inadequate for measuring metal abundances. A typical optical afterglow spectrum exhibits a wide range of ISM absorption features due to rest-frame UV transitions of low- and high-ionization metal species, which allow a direct determination of the column density of these elements along the GRB line of sight through the host galaxy. Combined with a determination of the neutral hydrogen column density via the Lyα line, it is possible to determine the ISM abundances (e.g., Berger et al. 2006; Prochaska et al. 2007; Fynbo et al. 2009).

Of the ions typically present in an afterglow spectrum, many are due to refractory elements and therefore depletion onto dust precludes their use as robust abundance indicators (they can be used to place a lower limit on the metallicity). In this work, we use S II, when available, as a measure of the metallicity, primarily since sulfur is not strongly depleted onto dust. Furthermore, the S II $\lambda\lambda$1250.6, 1253.8 transitions have low oscillator strengths, and the corresponding lines are more likely to be unsaturated.

In Table 3, we present a compilation of metallicities for our GRB host sample, including the spectral line used, the neutral hydrogen column density, and the column density of the metal ion computed using the measured equivalent width of the transition. All these values are taken from the literature (Hjorth et al. 2003; Vreeswijk et al. 2004; Cucchiara et al. 2006; Fynbo et al. 2006; Ferrero et al. 2009; Fynbo et al. 2009; Ledoux et al. 2009; Thöne et al. 2010) and have been placed on the solar abundance scale of Asplund et al. (2005). We place lower limits on the metallicity using Si II, Si IV, and C II detections reported by Fynbo et al. (2009).

Prochaska et al. (2008) found a correlation between the rest-frame equivalent width of Si II λ1526.7 and the metallicity of damped Lyα absorbers (DLAs) along lines of sight to quasars

Table 3
Metallicities from Afterglow Absorption Spectroscopy for GRB Host Galaxies at $z \sim 3$–5 in this Study

GRB	z	$\log(N_{\rm HI})$ ($\rm cm^{-2}$)	Ion	Rest Wavelength (Å)	Observed Equivalent Width[a] (Å)	$\log(N_{\rm Ion})$ ($\rm cm^{-2}$)	[Z/H][b]
020124	3.198	21.70 ± 0.20[c]	...	...	...	...	...
030323	3.372	21.90 ± 0.07[d]	S II	1253.8	...	15.84 ± 0.19[d]	-1.20 ± 0.20
			Si II	1526.7	0.75 ± 0.03	...	-2.0 ± 0.3[e]
050319	3.240	20.90 ± 0.20[a]	Si IV	1402.8	9 ± 3	>14.67	>−1.74
			Si II	1526.7	6 ± 3	...	-0.7 ± 0.3[e]
050502	3.793	...	...	...	...	...	...
050730	3.968	22.10 ± 0.10[a]	S II	1253.8	...	15.11 ± 0.04[f]	-2.13 ± 0.11
050814	5.77[g]	...	...	...	...	...	...
050908	3.344	17.60 ± 0.10[a]	C II	1334.5	0.62 ± 0.18	>13.85	>−0.14
			Si II	1526.7	1.85 ± 0.15	...	-1.5 ± 0.3[e]
060115	3.533	21.50 ± 0.10[a]	Si II	1526.7	6.3 ± 1.6	>14.72	>−2.29
			Si II	1526.7	6.3 ± 1.6	...	-0.7 ± 0.3[e]
060206	4.048	20.85 ± 0.10[a]	S II	various[h]	...	15.21 ± 0.03[i]	-0.78 ± 0.1
060210	3.913	21.55 ± 0.10[a]	S II	1253.8	...	>15.80[j]	>−0.89
			Si II	1526.7	18.04 ± 0.19	...	-0.1 ± 0.3[e]
060526	3.221	20.00 ± 0.15[a]	S II	various[h]	...	14.58 ± 0.25[k]	-0.57 ± 0.25[k]
			Si II	1526.7	3.3 ± 0.4	...	-1.1 ± 0.3[e]
060605	3.773	18.90 ± 0.40[l]	...	...	...	...	...
060607	3.075	16.95 ± 0.03[a]	...	...	...	...	...
060707	3.425	21.00 ± 0.20[a]	S II	1250.6	6.7 ± 1.3	>16.30	>0.16
			Si II	1526.7	10.2 ± 1.4	...	-0.4 ± 0.3[e]
060906	3.686	21.85 ± 0.10[a]	Si II	1526.7	2.2 ± 0.9	>14.25[a]	>−3.11
			Si II	1526.7	2.2 ± 0.9	...	-1.4 ± 0.3[e]
060926	3.206	22.60 ± 0.15[a]	Si II	1526.7	4 ± 1.1	>14.56	>−3.55
			Si II	1526.7	4 ± 1.1	...	-0.95 ± 0.3[e]
060927	5.464	22.50 ± 0.15[a]	Si II	1260.4	9 ± 4	>13.99	>−4.02
061110B	3.433	22.35 ± 0.10[a]	Si II	1304.4	6.9 ± 1.1	>15.04	>−2.82
			Si II	1526.7	3.2 ± 0.8	...	-1.1 ± 0.3[e]

Notes.
[a] Fynbo et al. (2009).
[b] Solar abundances are from Asplund et al. (2005). The metallicities have been re-derived from the quoted metal ion column densities, as necessary.
[c] Hjorth et al. (2003).
[d] Vreeswijk et al. (2004).
[e] Based on the Si II λ1526.7 equivalent-width–metallicity correlation for QSO-DLAs (Prochaska et al. 2008).
[f] Ledoux et al. (2009).
[g] This is a photometric redshift (Curran et al. 2008).
[h] Derived by simultaneous least-squares fitting of the S II λ1250.6, λ1253.8, and λ1259.5 transitions.
[i] Fynbo et al. (2006).
[j] Cucchiara et al. (2006).
[k] Thöne et al. (2010).
[l] Ferrero et al. (2009).

(QSO-DLAs). For comparison purposes, we also quote the metallicity as derived by applying this relation to our sample, where the uncertainty of 0.3 dex incorporates the scatter about the correlation as well as uncertainties in individual QSO-DLA metallicity measurements. We note that these estimates are at times inconsistent for individual GRBs where independent estimates (030323 and 060526) for or lower limits (060707) on the metallicity are available. However, it remains plausible (Section 4) that this relation may still trace the ensemble properties of the GRB-DLA sample, in addition to those of QSO-DLAs.

Finally, for five GRBs in our sample, metal line equivalent widths are not available and we do not consider them in our mass–metallicity analysis (Section 4). We also exclude GRB 050908, for which the H I column density is very low ($\log N_H = 17.6 \pm 0.1$; Fynbo et al. 2009), suggesting that the medium along the line of sight may not be mainly neutral. The same quantities for the five additional GRB hosts at $z \gtrsim 3$ from the literature are listed in Table 4.

3. OPTICAL LUMINOSITIES AND STELLAR MASSES OF LONG GRB HOSTS AT $z \sim 3$–5

Before we address the M_*–Z relation itself, we explore the rest-frame optical properties of our $z \sim 3$–5 long GRB host galaxy sample since this analysis has not been performed previously. We compare our sample to long GRB hosts at $z \lesssim 2$ to explore any evolution in host properties, as well as to field galaxy samples at similar redshifts to place the long-duration GRB hosts in a broader context.

3.1. Luminosity Distribution

Since the *Spitzer* 3.6 μm band probes different parts of the host SEDs at different redshifts (Figure 1), we must correct the inferred luminosities to a common rest-frame wavelength for a meaningful comparison (K-correction). Doing so requires knowledge of the host SED, which we do not have for our targets. We therefore employ evolutionary single stellar population (SSP) models with a single burst of star formation (e-folding

Table 4
Metallicities from Afterglow Absorption Spectroscopy for GRB Host Galaxies from Previous Studies

GRB	z	$\log(N_{\rm HI})$ ($\rm cm^{-2}$)	Ion	Rest Wavelength (Å)	Observed Equivalent Width (Å)	$\log(N_{\rm Ion})$ ($\rm cm^{-2}$)	[Z/H][a]
050904	6.295	≈ 21.6[b]	S II	1253.8	3.8 ± 1.1	15.6 ± 0.15[c]	$-1.14^{+0.14}_{-0.17}$
060223A	4.406	21.60 ± 0.10[d]	Si II	1304.4	...	≈ 15.3[d]	> -1.8
060510B	4.942	21.30 ± 0.10[d]	S II	1250.6, 1253.8	...	15.6 ± 0.1[d]	-0.85 ± 0.15
060522	5.110	21.00 ± 0.30[d]	...	...	...	...	...
080607	3.036	22.70 ± 0.04[e]	S II	1250.6	6.73 ± 0.27	> 16.3	> -1.5
			Si II	1526.7	7.85 ± 0.15	...	-0.5 ± 0.3[f]

Notes.
[a] Solar abundances are from Asplund et al. (2005). The metallicities have been re-derived from the quoted metal ion column densities, as necessary.
[b] Totani et al. (2006).
[c] Kawai et al. (2006).
[d] Chary et al. (2007) and Price et al. (2007).
[e] Prochaska et al. (2009).
[f] Based on the Si II λ1526.7 equivalent-width–metallicity correlation for QSO-DLAs (Prochaska et al. 2008).

time, $\tau = 0$) to determine the K-corrections. Leibler & Berger (2010) recently performed stellar population modeling of 23 long GRB hosts at $z \approx 0.03$–1.6 using multi-band photometry from Savaglio et al. (2009) and the evolutionary models of Maraston (2005). They determined a median stellar population age of $10^{-1.2\pm0.1}$ Gyr (see also Savaglio et al. 2009). Taking this age range into account, along with a Salpeter IMF, and a metallicity range of 0.05–0.5 $Z_\odot$, we find that the flux density of the SSP models in the rest-frame 0.4–2μm range is well approximated by a power law, $F_\lambda \propto \lambda^\beta$, with $\beta = -2.3 \pm 0.2$. This assumes negligible extinction, which is appropriate for most GRB host galaxies (Savaglio et al. 2009). Using this result as an estimate of the intrinsic spectrum of GRB hosts at $z \gtrsim 3$, we determine the host absolute magnitudes including K-correction as follows:

$$M_{\rm AB}(\lambda_0) = m_{\rm AB} - 5\log\left(\frac{d_{\rm L}}{10\ {\rm pc}}\right) - 2.5(\beta+2)\log\left[\frac{(1+z)\lambda_0}{\lambda}\right] + 2.5\log(1+z), \quad (2)$$

where $M_{\rm AB}$ is the absolute magnitude at a rest wavelength, λ_0, to which the K-correction is performed, d_L is the luminosity distance, and λ is the effective wavelength of the observed band (3.55 μm for our *Spitzer* observations). To minimize the K-corrections for our sample we select a nominal rest-frame wavelength, $\lambda_0 = 7800$ Å (Figure 1), roughly corresponding to the I band. The resulting mean K-correction on our photometry is about -1.7 mag (dominated by the last term on the right-hand side of Equation (2)), with a standard deviation of about 0.2 mag.

The resulting luminosity distribution for our sample is shown in Figure 5, and the inferred absolute magnitudes are listed in Table 1. Also included are the five host galaxies from the literature (their values are listed in Table 2). In the comparison to low-redshift GRB hosts and to field galaxies provided below we treat separately our uniform sample and the combined sample that includes the five hosts from the literature. For our detected hosts we find a range of $M_{\rm AB}(780\,{\rm nm}) \approx -21.5$ to -22.5 mag, while the limits are typically $M_{\rm AB}(780\,{\rm nm}) \gtrsim -20.4$ mag. The stack limit corresponds to $M_{\rm AB}(780\,{\rm nm}) \gtrsim -19.1$ mag. With less than a 50% detection fraction it is not possible to robustly estimate the median luminosity of our sample, but the formal 3σ upper limit is about -21.5 mag. The stack limit, however, suggests that a more reasonable upper bound on the median is about $M_{\rm AB}(780\,{\rm nm}) \gtrsim -19.1$ mag. The addition of the five hosts from the literature does not change this result.

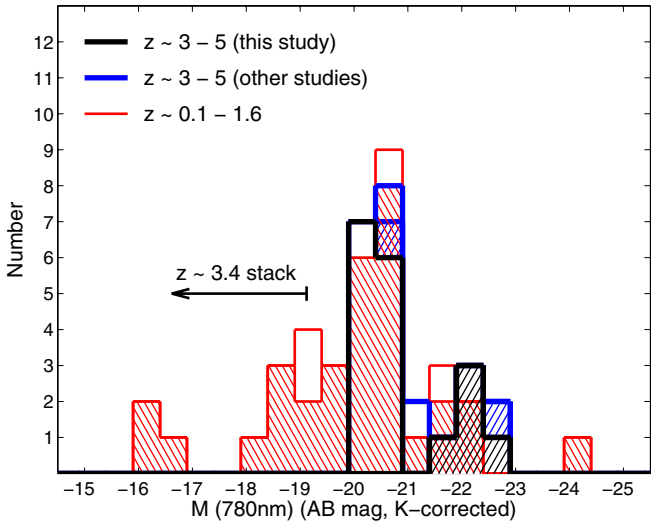

Figure 5. Luminosity distribution for GRB hosts at $z \sim 3$–5 from our study (black) and the five GRB hosts at $z \gtrsim 3$ from previous studies (blue; Berger et al. 2007; Chary et al. 2007; Chen et al. 2010), compared with GRB hosts at $z \sim 1$ (red). All samples have been K-corrected to 780 nm in the rest frame. Non-detections (3σ upper limits) are shown as open histograms. Also shown is the stack limit at a median redshift of $z \approx 3.4$.
(A color version of this figure is available in the online journal.)

3.1.1. Comparison with Long GRB Hosts at $z \lesssim 2$

To compare the resulting optical luminosity distribution to GRB hosts at low redshift, we obtain a comparison sample from ground-based *JHK* and *Hubble Space Telescope* 814 nm photometry reported in Castro Cerón et al. (2010) and Savaglio et al. (2009), and from our own GRB host follow-up studies. The comparison sample has a redshift range of $z \approx 0.01$–2 with a median of $z \approx 0.86$. For each host we select the band that corresponds most closely to a rest-frame wavelength of 7800 Å to minimize the K-corrections relative to our *Spitzer* sample. The mean and standard deviation of the resulting K-corrections are -0.6 and 0.3 mag, respectively.

The luminosity distribution for the low-redshift sample is shown in Figure 5. There is clear overlap between the two GRB host samples at the bright end, but due to the lower redshifts

Table 5
Field Galaxy Comparison Samples

Sample	z	$\langle z \rangle$	Detections	Limits	$\langle m_{\rm AB} \rangle$[a] (mag)	$\langle M_{\rm AB} \rangle$[b] (mag)	Depth (mag)
Reddy et al. (2006)	$2.29 \leqslant z \leqslant 3.00$	2.94	32	6	23.2	−22.2	24.9
Reddy et al. (2006)	$3.00 \leqslant z \leqslant 3.66$	3.22	31	5	23.7	−21.9	24.9
Magdis et al. (2010)	$2.34 \leqslant z \leqslant 3.00$	2.93	19	3	23.4	−22.0	25.5
Magdis et al. (2010)	$3.00 \leqslant z \leqslant 3.45$	3.20	30	6	23.6	−22.0	25.5
Shapley et al. (2005)	$1.48 \leqslant z \leqslant 2.90$	2.30	72	0	22.8	−22.1	$R < 25.5$
Ono et al. (2010)	3.1, 3.7[c]	3.40	11	261	23.7	−22.1	24.8
This work	$3.0 \leqslant z \leqslant 5.8$	3.43	5	13	23.8	−22.0	24.8[d]

Notes.
[a] Median apparent magnitudes in the *Spitzer* 3.6 μm band (Reddy et al. 2006; Magdis et al. 2010; Ono et al. 2010) and *K* band (Shapley et al. 2005).
[b] Corresponding median absolute magnitudes.
[c] This work on LAEs uses two narrowband filters tuned to Lyα at $z \sim 3.1$ and $z \sim 3.7$.
[d] Median apparent magnitude of our 3.6 μm non-detections.

of the comparison sample, its luminosity distribution extends to much fainter levels (reaching ≈ -16.5 mag), with a median of about $-20.1^{+0.9}_{-0.4}$ mag (95% confidence range). This is consistent with the upper bound on the median luminosity of our $z \sim 3$–5 sample. Indeed, a log-rank test including the individual non-detections indicates that the hypothesis that $z > 3$ and $z \sim 1$ samples are drawn from the same underlying population has a p-value of 0.92. Similarly, the fraction of detected hosts above our threshold of $M_{\rm AB}(780\,{\rm nm}) \approx -21.5$ mag is about 1/4 for both samples. Finally, our stack non-detection level of $M_{\rm AB}(780\,{\rm nm}) \gtrsim -19.1$ mag is consistent with the median of the $z \sim 1$ GRB sample. Thus, we find no evidence for significant evolution in the optical luminosity function of GRB hosts from $z \sim 1$ to ∼4. We note that dividing the comparison sample into $z < 1$ and $z > 1$ subsets does not change this result.

3.1.2. Comparison with Lyman-break Galaxies and Lyα Emitters

To assess whether the luminosities we find for GRB hosts at $z \gtrsim 3$ are typical of field galaxies, we next compare the resulting luminosity distribution with other galaxy samples at similar redshifts: Lyman-break galaxies (LBGs) and Lyα emitters (LAEs). For the LBG comparison we use *Spitzer* 3.6 μm photometry in the GOODS-N field reported by Reddy et al. (2006) and Magdis et al. (2010), based on deep (∼95 hr) *Spitzer* observations. We also include a sample of 72 star-forming galaxies at $z \sim 2.3 \pm 0.3$ from Shapley et al. (2005) selected based on their rest-frame UV brightness. The resulting luminosity distributions for these samples are shown in Figure 6, and their summary statistics are listed in Table 5. *K*-corrections for the SED shape (the third term on the right-hand side of Equation (2)) have not been applied to any of the samples, although the difference between the *K*-corrections should be minor ($\lesssim$0.2 mag) and would not modify the shape of the distributions.

Our GRB host sample is clearly missing the luminous tail of LBGs at $M_{\rm AB} \lesssim -23$ mag, which accounts for ≈20% of the comparison samples. The median absolute magnitude of the LBG sample is $-22.0^{+0.3}_{-0.2}$ mag for Reddy et al. (2006) and $-21.9^{+0.5}_{-0.2}$ mag for Magdis et al. (2010) (95% confidence ranges), brighter than the 3σ upper limit for the GRB sample (−21.5 mag, without *K*-corrections for the SED shape) and our stack limit. A log-rank test yields a p-value of 0.04 and 0.09 that the GRB host sample (including the five hosts from other studies) is drawn from the same population as the parent population of the LBG samples of Reddy et al. (2006) and Magdis et al. (2010), respectively. It is important to note, however, that since the LBG sample is flux limited (based on the initial rest-frame UV selection and spectroscopic confirmation), whereas the GRB host sample is not, we cannot simply use the fractional detections of LBGs as an indication of the overall luminosity function.

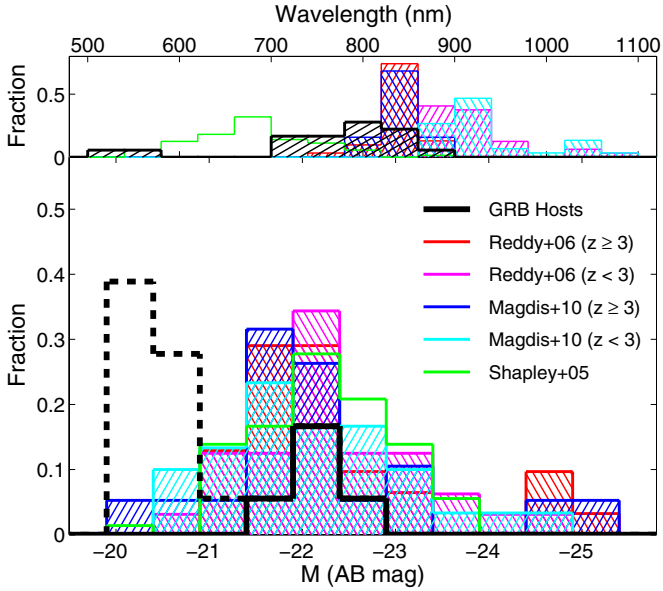

Figure 6. Normalized luminosity distribution for the GRB hosts in our sample (black: solid = detections; dashed = limits) compared with LBGs at $z \sim 3$. Reddy et al. (2006) and Magdis et al. (2010) use *Spitzer* 3.6 μm observations of GOODS-N and probe deeper than our study (Table 5), while Shapley et al. (2005) rely on ground-based *K*-band photometry. *K*-corrections for the SED shape (last term in Equation (2)) have not been applied (although the relative difference in *K*-correction should be minor and will not modify the shape of the distribution). Non-detections have been removed from the comparison samples for clarity. The upper panel shows the corresponding distributions of the rest-frame wavelengths for each sample.
(A color version of this figure is available in the online journal.)

To further assess whether the dearth of GRB hosts with $M_{\rm AB} \lesssim -23$ mag in our sample is significant, we instead need to integrate the rest-frame optical luminosity function. This will allow us to assess the expected fraction of GRB hosts with $M_{\rm AB} \lesssim -23$ mag compared to our threshold of about −21 mag. Marchesini et al. (2007) calculated a Schechter fit to the *V*-band luminosity function at

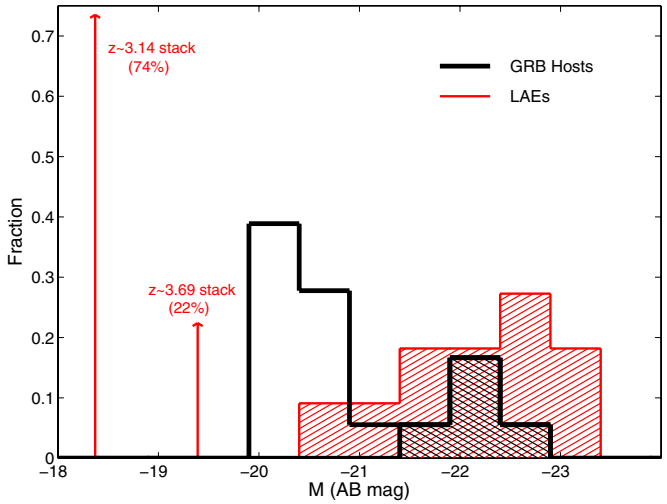

Figure 7. Same as Figure 6, but compared with *Spitzer* 3.6 μm observations of Lyα emitters at $z \sim 3.1$ and $\sim$3.7 (red; Ono et al. 2010). Only 4% of the LAE sample was detected individually (red histogram), while stacks at $z \sim 3.1$ and $\sim$3.7 revealed much lower typical luminosities of $M_{\rm AB} \approx -18.3$ mag and ≈ -19.4 mag, respectively. *K*-corrections for the SED shape (last term in Equation (2)) have not been applied (although the relative difference in *K*-correction should be minor and will not modify the shape of the distribution).

(A color version of this figure is available in the online journal.)

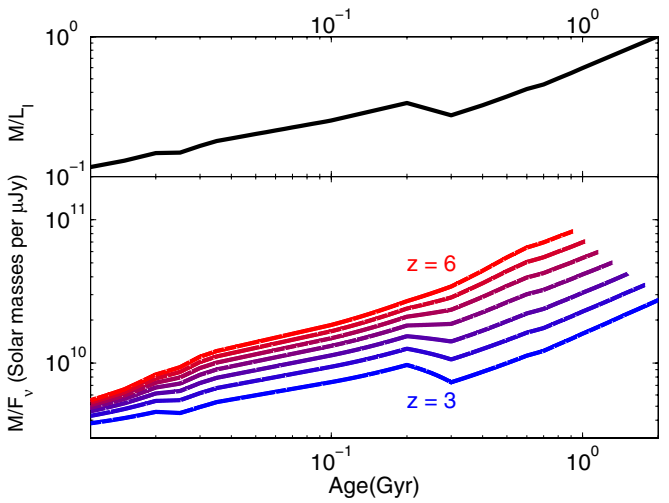

Figure 8. Upper panel: mass-to-light ratio in the rest-frame *I* band from the Maraston (2005) simple stellar population models in solar units. The models assume an instantaneous burst of star formation ($\tau = 0$). Lower panel: ratio of stellar mass to observed 3.6 μm flux density for ($\tau = 0$) SSP models as a function of age at different redshifts from $z = 3$ (bottom curve) to $z = 6$ (top curve) in steps of $\delta z = 0.5$. The models used in this paper are for a Salpeter IMF with a red horizontal branch morphology and a metallicity of 0.02 $Z_\odot$. Each curve is truncated at a value that corresponds to the age of the universe at that redshift.

(A color version of this figure is available in the online journal.)

$z \sim 3$ and found $M^*_{\rm AB}(V) = -22.77 \pm 0.22$ mag and faint-end slope, $\alpha = -1.12 \pm 0.24$. Applying a *K*-correction from the *V* to *I* band using $F_\lambda \propto \lambda^{-2.3\pm0.2}$ (Section 3.1) we find $M^*_{\rm AB}(I) = -22.65 \pm 0.30$ mag. Assuming that α is the same in the *I* band as in the *V* band, we find that about 10% of our sample (or about two hosts) should have $M_{\rm AB} \lesssim -23$ mag if the GRB hosts are drawn from the field galaxy population.[7] Since this small number is fully consistent with zero detections, we cannot rule out the hypothesis that GRB hosts are drawn from the general LBG population. Since the LBG sample is rest-frame UV-selected, a more thorough analysis of the relation between the optical luminosity functions of GRB hosts and LBGs requires an understanding of the relation between the UV and optical luminosities of LBGs, which is currently not available.

For the comparison to LAEs we use the sample of Ono et al. (2010), which includes 205 LAEs at $z \sim 3.1$ and 67 LAEs at $z \sim 3.7$ with multi-band photometry. These authors find 11 detections at 3.6 μm (5 at $z \sim 3.1$ and 6 at $z \sim 3.7$), corresponding to a detected fraction of only 4%. From a stacking analysis of the non-detected LAEs they determine $\langle M_{\rm AB} \rangle = -20.8$ mag at $z \approx 3.1$ and $\langle M_{\rm AB} \rangle = -21.1$ mag at $z \approx 3.7$. A comparison between the GRB hosts and LAEs at $z \sim 3.1$–3.7 is shown in Figure 7. The luminosity distributions of the detected LAEs and GRB hosts appear to be consistent. However, including the LAE non-detections and carrying out a log-rank test we find a negligible probability that the GRB host sample is drawn from the same population as the LAE sample at $z \sim 3.4$ since our sample has a much higher detection fraction than the LAEs. This is an interesting result since several GRB hosts have been previously detected as LAEs (e.g., Fynbo et al. 2002, 2003; Jakobsson et al. 2005). It suggests that GRBs select the more luminous end of the LAE luminosity distribution.

[7] We verify this approach by calculating the expected fraction of galaxies with $M_{\rm AB} \lesssim -23$ mag for our various comparison samples. We find that relative to their typical threshold absolute magnitude of about -21.5 to -22 mag (Figure 6), this expected fraction is about 20%, which is in good agreement with the observed fraction.

To conclude, the comparisons to LBGs and LAEs suggest that GRB hosts at $z \gtrsim 3$ are currently missing the bright end of the LBG luminosity distribution (with the exception of the host of GRB 080607), but that this may be due to the small sample size. On the other hand, GRB hosts sample the high end of the LAE luminosity distribution.

3.2. Stellar Mass Distribution

We next turn to a derivation of the stellar masses of our GRB host sample. Computing stellar masses from observed luminosities in a given wave band requires knowledge of the mass-to-light ratio and hence the stellar population age and metallicity. When multi-band photometry is available, modeling of the SED using stellar population synthesis models can be used to determine stellar masses, provided that an SSP is assumed. When multi-band photometry is not available, the resulting uncertainty in the mass-to-light ratio (e.g., at $\sim$1 μm) is about an order of magnitude (e.g., Magdis et al. 2010).

Here, since we lack broadband photometry, we determine a range of mass-to-light ratios for each galaxy in the observed 3.6 μm band using a wide range of population ages and the SSP models of Maraston (2005) with a Salpeter IMF. We assume an instantaneous burst of star formation ($\tau = 0$). As expected, the 3.6 μm mass-to-light ratio for these models increases with stellar population age beyond $\sim$10 Myr. This is shown in Figure 8, where the ratio of the stellar mass to the observed flux density at 3.6 μm is plotted as a function of age and redshift. The more traditional mass-to-light ratio in solar units (in the rest-frame *I* band) is also plotted for comparison. The upper bound on the mass-to-light ratio is achieved by setting the stellar population age to the age of the universe at each host redshift ($\approx$1.8 Gyr at the median redshift of our sample). We stress that this leads to a very conservative maximum mass for each host galaxy since studies of LBGs and LAEs indicate typical population ages of $\sim$0.1–0.6 Gyr (Shapley et al. 2005; Reddy et al. 2006; Magdis

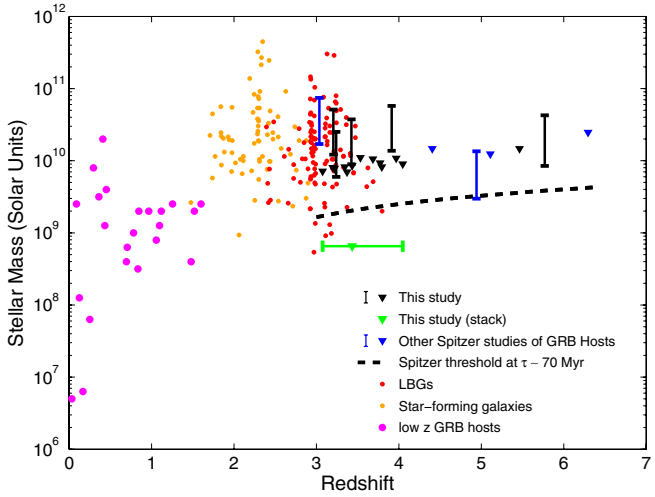

Figure 9. Stellar masses plotted as a function of redshift for our sample (black). Bars indicate detections with the upper and lower ends defined by the maximal mass-to-light ratio and a 70 Myr old stellar population, respectively. Individual limits (triangles) are plotted for the maximal masses, while the dashed curve indicates the 3σ limit ($0.25\,\mu$Jy) for a 70 Myr old stellar population. The stack limit for 11 non-detections at $z \approx 3.4$ is designated by the triangle and horizontal bar (70 Myr old population). Also shown are the five previous *Spitzer* observations at $z \gtrsim 3$ from the literature (blue symbols) and low-redshift GRB hosts from the study of Leibler & Berger (2010). The additional comparison samples include star-forming galaxies at $z \sim 2$ (orange; Shapley et al. 2005) and LBGs at $z \sim 3$ (red; Reddy et al. 2006; Maiolino et al. 2008; Mannucci et al. 2009; Magdis et al. 2010). The *Spitzer*-detected GRB hosts at $z \sim 3$–5 have similar masses to the most massive GRB hosts at $z \sim 1$ and to the LBGs at $z \sim 3$. The stack limit is similar to the typical masses of GRB hosts at $z \sim 1$.

(A color version of this figure is available in the online journal.)

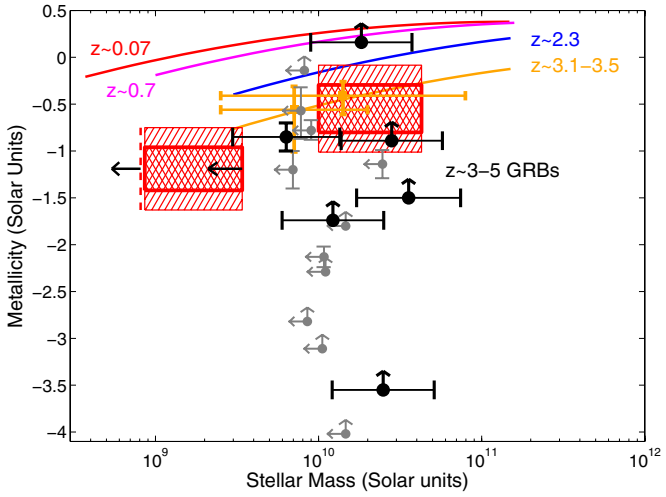

Figure 10. Stellar mass plotted as a function of ISM metallicity for our sample and the five previously observed hosts (black = detections; gray = limits). The red hatched regions designate 1σ and 2σ intervals for estimates of the mean metallicity at two mass bins of $\sim 2 \times 10^{10}\,M_\odot$ ($3.6\,\mu$m detections) and $\lesssim 3.4 \times 10^9\,M_\odot$ (scaled stack limit—see the text). The red dashed vertical line indicates the upper limit on the mean mass of the stack for a 70 Myr population. Where only metallicity lower limits were available, a conservative upper limit of $2\,Z_\odot$ was assumed. These data are consistent with a decline in metallicity with lower stellar mass—an M_*–Z relation. Also shown are the relations for $z \sim 0.07$ (Kewley & Ellison 2008), $z \sim 0.7$ (Savaglio et al. 2005), $z \sim 2.3$ (Erb et al. 2006), and $z \sim 3.1$–3.5 (Maiolino et al. 2008; Mannucci et al. 2009, filled squares); the relations at $z \lesssim 2.3$ are the re-calibrated values by Maiolino et al. (2008). Our two data regions at $z \sim 3$–5 fall below these relations suggesting that the M_*–Z relation continues to evolve to $z \sim 4$.

(A color version of this figure is available in the online journal.)

et al. 2010; Ono et al. 2010). For a more typical age we adopt the median age for long GRB hosts at $z \sim 1$ of about 70 Myr (Leibler & Berger 2010). The variation in mass-to-light ratio between these age values is about an order of magnitude, as expected from other galaxy studies. The 70 Myr and maximum mass-to-light ratios are listed in Table 1 for our sample, and in Table 2 for the five hosts from the literature.

We test the effect of metallicity on the mass-to-light ratio by considering population synthesis models at 0.02 and 0.5 $Z_\odot$, which cover the typical range of GRB host galaxy metallicities. The resulting variation in the mass-to-light ratio is only $\sim$15%, with the lower metallicity models typically yielding systematically smaller values (although this effect is redshift-dependent). This is a much smaller effect than the uncertainty due to the unknown stellar population age. In the following, we adopt the mass-to-light ratios for a metallicity of 0.02 $Z_\odot$.

The inferred masses of our GRB host sample are plotted as a function of redshift in Figure 9 and are listed in Table 1. The maximal masses inferred for our sample are (2.5–5.8) $\times$ $10^{10}\,M_\odot$, while the typical (maximal) upper limits are $\lesssim 9 \times 10^9\,M_\odot$. The masses inferred for a 70 Myr old population are about (0.6–1.4) $\times$ $10^{10}\,M_\odot$, with typical upper limits of $\lesssim 2 \times 10^9\,M_\odot$. The mass limit from the stack of 11 GRB hosts is $\lesssim 7 \times 10^8\,M_\odot$ for a 70 Myr old population and $\lesssim 3 \times 10^9\,M_\odot$ for the maximal age. We also consider the previous five long GRB hosts at $z \gtrsim 3$ (Table 2), including two detections with maximal masses of $1.4 \times 10^{10}\,M_\odot$ (GRB 060510B; Chary et al. 2007) and $7.4 \times 10^{10}\,M_\odot$ (GRB 080607; Chen et al. 2010) in our M_*–Z analysis.

In comparison to these values, the typical stellar mass of the $z \sim 1$ GRB host sample is about $1.2 \times 10^9\,M_\odot$, similar to our stack limit. Similarly, the most massive GRB hosts at $z \sim 1$ have masses of $\sim 10^{10}\,M_\odot$, similar to our detected hosts. We reach a similar conclusion in comparison to the LBG sample at $z \sim 3$: the typical stellar masses of the *Spitzer*-detected LBGs (Reddy et al. 2006; Magdis et al. 2010) are about $10^{10} M_\odot$, although some of these galaxies ($\sim$5%) have stellar masses in excess of $10^{11}\,M_\odot$. This is similar to the distribution of our detected hosts and the five literature hosts. Our stack (maximal) limit falls below the typical stellar mass detection limit of the LBG sample. However, in the absence of a detailed mass function, it is difficult to estimate how the flux limit associated with the LBG selection compares to our detected fraction. Regardless of the exact answer, it is clear that deeper observations of the GRB host sample will probe lower mass systems than available with the LBG sample.

4. THE MASS–METALLICITY RELATION AT $z \sim 3$–5

We now turn to the primary investigation of this paper—the M_*–Z relation at $z \sim 3$–5. In Figure 10, we present the absorption-line metallicities plotted versus the stellar masses inferred from our *Spitzer* observations ("our sample"). Also included are the five GRB hosts from previous targeted observations ("literature sample," Table 4). Of the 18 GRBs in our sample, four (GRBs 030323, 050730, 060206, and 060526) have determined [S/H] values, two (060210 and 060707) have lower limits on their metallicity from a potentially saturated S II line, six have lower limits based on Si II or Si IV detections, and six have no metallicity information. For the literature sample, the spectrum of GRB 080607 exhibits a saturated S II line, leading to a lower limit on the metallicity; GRB 060223A has a lower limit based on an Si II detection; GRBs 060510B and

050904 have measured metallicities; and GRB 060522 has no metallicity information.

Using these values we find a wide range of metallicities[8] spanning up to three orders of magnitude for the *Spitzer*-detected GRB hosts, which have stellar masses of $\sim 2 \times 10^{10}\,M_{\odot}$. This range indicates that at least some of the hosts have metallicities that are typical of $z \sim 1$–2 galaxies in the same mass range. We note that this range is significantly larger than the scatter in metallicity observed at low redshift, which is about 0.4 dex at $\log M_{*} \sim 10$ (Tremonti et al. 2004). Since GRBs probe the metallicities of their host galaxies along random lines of sight (whereas direct galaxy spectroscopic observations yield luminosity-weighted metallicities), this larger scatter may be indicative of the intrinsic scatter in the metallicities of individual star-forming regions in $z \gtrsim 3$ galaxies. We return to this point in Section 5.

To search for an M_{*}–Z relation, we divide the GRBs with available metallicity information into two mass bins—the 3.6 μm detections with $M_{*} \sim 2 \times 10^{10}\,M_{\odot}$ (Group 1: GRBs 050319, 060210, 060510B, 060707, 060926, and 080607) and the objects included in the stack (Group 2: GRBs 030323, 050730, 060115, 060206, 060526, 060906, and 061110B). For each group, we perform a Monte Carlo simulation to estimate the mean metallicity. We represent metallicity detections by Gaussian random variables with a mean equal to the detected metallicity and variance equal to the observed uncertainty. For objects with only lower limits, we assume an upper bound of two times solar,[9] and represent the resulting metallicity ranges by uniform distributions. The simulations yield nearly Gaussian distributions for the mean metallicity of objects in both bins, with $\langle Z_1 \rangle = -0.55 \pm 0.24$ and $\langle Z_2 \rangle = -1.19 \pm 0.22$, where the quoted uncertainties are 1σ errors on the mean. The mean metallicities of the two groups are different at the level of about 2.7σ. Repeating this analysis using metallicities derived from the Si II λ1526.7 equivalent-width–metallicity correlation (Prochaska et al. 2008) yields a similar result, with $\langle Z_1 \rangle = -0.50 \pm 0.12$ and $\langle Z_2 \rangle = -1.13 \pm 0.09$ (Figure 11).

For Group 1, the mean of the maximum inferred stellar masses is $4.3 \times 10^{10}\,M_{\odot}$, while that of the masses inferred from the 70 Myr populations is $1.0 \times 10^{10}\,M_{\odot}$. To obtain mass estimates for Group 2, we scale our stack limit obtained for 11 non-detections by $\sqrt{11/7}$. Using the mean maximum mass-to-light ratio of the objects in Group 2 ($3.7 \times 10^{10}\,M_{\odot}\,\mu\mathrm{Jy}^{-1}$) yields an upper limit on the mean stellar mass of these seven objects of $<3.7 \times 10^{9}\,M_{\odot}$, while the mean mass-to-light ratio at 70 Myr ($8.4 \times 10^{9}\,M_{\odot}\,\mu\mathrm{Jy}^{-1}$) yields a mass limit of $<8.4 \times 10^{8}\,M_{\odot}$. The resulting mass ranges together with the corresponding 1σ and 2σ metallicity ranges for both groups are indicated by hatched regions in Figure 10. We find that the mean metallicity decreases as a function of stellar mass, an initial indication of an M_{*}–Z relation. We note that our averaging of the individual metallicities at a fixed stellar mass is similar to the approach taken by Erb et al. (2006) for their $z \sim 2.3$ sample for which they constructed composite spectra in various mass bins (i.e., they averaged the spectra, while we average the individual metallicities).

To compare our measurements with the observed M_{*}–Z relations at lower redshifts, we need to ensure the use of a common stellar IMF and calibration of the spectral indices used to measure the metallicities. We use the results of Maiolino et al. (2008) who re-calibrated the $z \sim 0.07$ relation of Kewley & Ellison (2008), the $z \sim 1$ relation of Savaglio et al. (2005), and the $z \sim 2.3$ relation of Erb et al. (2006) to the Salpeter IMF. In Figure 10, we plot the resulting M_{*}–Z relations given in Maiolino et al. (2008), which are of the form

$$Z \equiv [\mathrm{O/H}] = -0.0864\,(\log M_{*} - \log M_{0})^{2} + K_{0} - (\mathrm{O/H})_{\odot}, \quad (3)$$

where M_0 and K_0 are the parameters of the log-parabolic fit to the re-calibrated data, and $(\mathrm{O/H})_{\odot} = 8.66$ is the solar oxygen abundance (Asplund et al. 2005). We also include in Figure 10 the M_{*}–Z relation inferred for LBGs at $z \sim 3.1$–3.5 (Maiolino et al. 2008; Mannucci et al. 2009), along with the mean M_{*}–Z points for $z \sim 3.1$ (Mannucci et al. 2009) and $z \sim 3.5$ (Maiolino et al. 2008). We find that our two points fall below the observed relations at $z \lesssim 3.5$, providing tentative evidence that the galaxy M_{*}–Z relation continues to evolve at $z \sim 3$–5, with our stack range probing a somewhat lower mass scale than the LBG studies at $z \sim 3.1$–3.5.

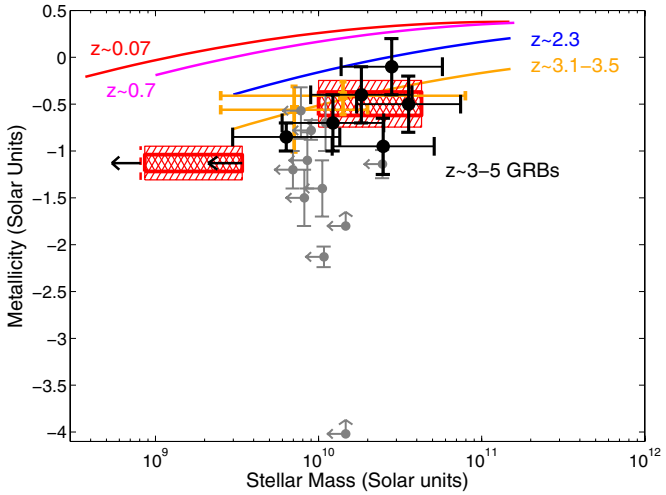

Figure 11. Same as Figure 10, except the metallicity lower limits have been replaced by estimates (where available) using a correlation between Si II λ1526.7 equivalent width and metallicity found for QSO-DLAs (Prochaska et al. 2008). (A color version of this figure is available in the online journal.)

5. DISCUSSION AND CONCLUSIONS

We present the first study of the galaxy mass–metallicity relation at redshifts of $z \sim 3$–5 using GRB afterglow absorption metallicities and *Spitzer* follow-up observations. Five of the twenty GRB hosts in our sample are detected above a 3σ flux density threshold of 0.25 μJy, corresponding to a typical stellar mass of $\sim 2 \times 10^{10}\,M_{\odot}$. We further place a limit of $\lesssim 3 \times 10^{9}\,M_{\odot}$ on the non-detected hosts based on a stacking analysis.

The rest-frame optical luminosities and derived masses are generally similar to those found for GRB hosts at lower redshifts, but are larger than for LAEs at similar redshifts. The comparison to the LBG population is less certain. No GRB hosts in our sample are detected with $M_{\mathrm{AB}} \lesssim -23$ mag, while about 20% of the LBG sample are more luminous than this value. On the other hand, integration of the $z \sim 3$ optical luminosity function suggests that we expect only $\sim$2 GRB hosts brighter than this limit in our sample, statistically consistent with zero detections.

Our sample focuses on GRBs with detected optical afterglows. This may raise the concern that we are missing highly extincted events, which may preferentially lie in high-metallicity

[8] To transform the sulfur and oxygen abundances we use the solar values listed in Asplund et al. (2005).

[9] These results are relatively insensitive to the choice of upper bound; placing one at 5 $Z_{\odot}$ instead of at 2 $Z_{\odot}$, increases the estimates of the means by $\sim$25%.

environments, thereby biasing our sample to low metallicities. Whereas there is some evidence that host galaxies of the so-called dark bursts at $z \lesssim 0.5$ could be in high-metallicity environments (Levesque et al. 2010b), there is no evidence for the same at high redshift. In fact, the hosts of high-redshift dark bursts appear to have similar optical colors and luminosities as those with detected optical afterglows (Perley et al. 2009), while radio and millimeter observations, which probe obscured star formation, indicate similar star formation rates (SFR) for both types of GRB hosts (Berger et al. 2003; Tanvir et al. 2004; Castro-Tirado et al. 2007). As a case in point, GRB 080607 is an example of such a dark burst, with a host galaxy stellar mass typical of GRB hosts at $z \gtrsim 3$ (Chen et al. 2010).

We find a wide dispersion in the metallicities of the host galaxies (inferred mainly from S II) at a fixed stellar mass of $\sim 2 \times 10^{10}\,M_{\odot}$. The mean metallicity at this mass scale is about $0.3\,Z_{\odot}$. The mean metallicity associated with 7 of the 11 non-detected hosts, which have an upper limit of $\lesssim 3.7 \times 10^{9}\,M_{\odot}$, is $Z \lesssim 0.1\,Z_{\odot}$. Thus, there appears to be an overall decline in metallicity with decreasing stellar mass, a hint of an M_{*}–Z relation. Furthermore, our two points on the M_{*}–Z relation lie below the relations at lower redshifts, suggesting that the relation continues to evolve at least to $z \sim 4$. Clearly, additional observations are required to confirm and increase the statistical significance of this result. A sample of 20 additional GRBs at $z \gtrsim 3$ from 2007 through the present is available for study. This will allow us to double the existing sample.

The observed range in metallicities at $M_{*} \sim 2 \times 10^{10}\,M_{\odot}$ appears to be larger than the observed scatter in metallicities at similar stellar masses in the nearby universe. While it is possible that this is a real effect, we caution that this may be an observational artifact; GRBs probe individual sight lines through their host galaxies, whereas traditional methods integrate the spectrum over an aperture or slit, thereby averaging over many individual H II regions (weighted by their luminosity). Since we divide galaxies into two groups and compute their mean metallicities, in effect we achieve a similar result as integrating over the many H II regions in individual galaxies.

Recent studies indicate an important third dimension in the galaxy M_{*}–Z relation—the SFR (Mannucci et al. 2010; Kocevski & West 2011). Systems with higher absolute SFR at a given stellar mass have systematically lower metallicities and therefore lie below the mean M_{*}–Z relation for their redshift. This effect is seen for GRB host galaxies at $z < 1$, which have high SFRs compared to field galaxies (Levesque et al. 2010a; Kocevski & West 2011). It would therefore appear plausible that the M_{*}–Z relation for GRB host galaxies at $z \sim 3$–5 presented here may appear different from that of the comparison samples at lower redshift, not due to a redshift evolution, but due to higher SFRs in the GRB hosts. To address this, we contrast the M_{*}–Z relation from GRB hosts as determined here to that for LBGs at $z \sim 3$ (Maiolino et al. 2008). Since the LBG sample comprises galaxies with the highest UV luminosities, and correspondingly, SFR at $z \sim 3$ (a few tens to hundreds of $M_{\odot}\,\mathrm{yr}^{-1}$; Maiolino et al. 2008; Mannucci et al. 2009), we would expect the M_{*}–Z relation as traced by LBGs to lie below the GRB sample, with typical SFR $\sim$ a few to tens of $M_{\odot}\,\mathrm{yr}^{-1}$ at $z \sim 1$ (Christensen et al. 2004; Savaglio et al. 2009). This is the opposite sense of what we find here, indicating that the observed evolution in the M_{*}–Z relation with redshift is likely real, and not due to variations in the SFR.

We end this article with some cautionary notes and future prospects. One possible source of systematic uncertainty in metallicities as probed by GRBs lies in the radial abundance profile of the host galaxies. The Milky Way and M33 display a strong abundance gradient (~ -0.07 dex kpc^{-1}: Rolleston et al. 2000; Cioni 2009). Similar abundance gradients (~ -0.05 dex kpc^{-1}) have been found for H II regions in nearby spiral galaxies (e.g., Vila-Costas & Edmunds 1992; van Zee et al. 1998). At higher redshift, Jones et al. (2010) find a gradient of -0.3 dex kpc^{-1} in a lensed system at $z = 2.0$; while this gradient is large in absolute terms, they clarify that it is similar to gradients in nearby spirals when the evolution of the effective radius out to $z \sim 2$ is taken into account. On the other hand, the LMC and SMC, which may be more representative of GRB hosts, display almost no radial metallicity gradient (Cioni 2009). Since GRBs probe an unknown line of sight through their hosts, a strong metallicity gradient combined with a preferred location for the progenitors may lead to a systematic bias in the resulting metallicity measurements. However, a distribution of GRBs that uniformly samples H II regions within their hosts, coupled with the potential that low-mass galaxies at high redshift have weak gradients, will negate such a bias.

We note that a similar effect may exist in direct galaxy metallicity measurements. This is simply because the measured metallicity is effectively a luminosity-weighted value, which therefore depends on the combined radial distribution and luminosities of H II regions. For example, if H II regions in the outskirts of LBGs were more luminous, an abundance gradient would lead to a biased metallicity value. Thus, assuming that galaxies of similar masses have similar abundance profiles, we would expect metallicities determined by GRBs as an ensemble for a given galaxy mass to be representative of the typical galaxy metallicity at that mass. We conclude that the effect of metallicity gradients is minimal when comparing samples as a function of galaxy mass.

A second concern is the relative calibration of absorption metallicities (using mainly the sulfur abundance) and nebular emission-line metallicities (using mainly the oxygen abundance). At present, the uncertainty in the solar abundance of these two elements (primarily oxygen) leads to at least $\sim$0.1 dex uncertainty in the relative calibration. Beyond this problem, an additional concern is that while to first order GRB absorption spectra and nebular lines both trace regions of star formation, it is unclear how the luminosity-weighted nebular metallicities relate in detail to the line-of-sight GRB metallicities (even in the absence of metallicity gradients). Thus, cross-calibration of the metallicities using direct spectroscopy of GRB hosts is of the utmost importance. This is missing at present.

Looking beyond additional *Spitzer* observations of existing GRB hosts, which from our work appear to have a detection yield of $\sim$25% at $z \gtrsim 3$, the *James Webb Space Telescope* (*JWST*) will provide a much deeper view of the M_{*}–Z relation at high redshift. For instance, the NIRCam instrument on *JWST* employing the $3.6\,\mu$m wide filter will be able to detect point sources at a 5σ flux of about 10 nJy in a similar integration time to our existing observations. This will allow us to detect GRB hosts at $z \sim 3$ down to a mass of $\sim 10^{8}\,M_{\odot}$ and at $z \sim 6$ to $\sim 3 \times 10^{8}\,M_{\odot}$. At these limits, we should be able to detect the bulk of the hosts individually if they are similar to GRB hosts at $z \sim 1$. Equally important, the NIRSpec instrument (1–5 μm) will allow us to determine emission-line metallicities for some of the hosts, and hence to cross-calibrate the afterglow absorption metallicities. Thus, with ongoing afterglow absorption metallicity measurements, the

GRB sample will continue to play a key role in our study of high-redshift galaxies.

We thank the anonymous referee for useful comments, which improved the quality of the manuscript. This work is based on observations made with the *Spitzer Space Telescope*, which is operated by the Jet Propulsion Laboratory, California Institute of Technology under a contract with NASA. Support for this work was provided by NASA through an award issued by JPL/Caltech.

REFERENCES

Asari, N. V., Cid Fernandes, R., Stasińska, G., et al. 2007, MNRAS, 381, 263
Asplund, M., Grevesse, N., & Sauval, A. J. 2005, in ASP Conf. Ser. 336, Cosmic Abundances as Records of Stellar Evolution and Nucleosynthesis, ed. T. G. Barnes III & F. N. Bash (San Francisco, CA: ASP), 25
Berger, E., Chary, R., Cowie, L. L., et al. 2007, ApJ, 665, 102
Berger, E., Cowie, L. L., Kulkarni, S. R., et al. 2003, ApJ, 588, 99
Berger, E., Penprase, B. E., Cenko, S. B., et al. 2006, ApJ, 642, 979
Blake, C., & Bloom, J. S. 2005, GCN Circ., 3327, 1
Bloom, J. S., Kulkarni, S. R., & Djorgovski, S. G. 2002, AJ, 123, 1111
Castro Cerón, J. M., Michałowski, M. J., Hjorth, J. M., et al. 2010, ApJ, 721, 1919
Castro-Tirado, A. J., Bremer, M., McBreen, S., et al. 2007, A&A, 475, 101
Chary, R., Berger, E., & Cowie, L. 2007, ApJ, 671, 272
Chen, H.-W., Perley, D. A., Wilson, C. D., et al. 2010, ApJ, 723, L218 (erratum 727, L53 [2011])
Christensen, L., Hjorth, J., & Gorosabel, J. 2004, A&A, 425, 913
Cioni, M. 2009, A&A, 506, 1137
Cucchiara, A., Fox, D. B., Penprase, B. E., et al. 2006, Nuovo Cimento B, 121, 1455
Curran, P. A., Wijers, R. A. M. J., Heemskerk, M. H. M., et al. 2008, A&A, 490, 1047
Diolaiti, E., Bendinelli, O., Bonaccini, D., et al. 2000, ApJ, 147, 335
Erb, D. K., Shapley, A. E., Pettini, M., et al. 2006, ApJ, 644, 813
Fazio, G. G., Hora, J. L., Allen, L. E., et al. 2004, ApJS, 154, 10
Ferrero, P., Klose, S., Kann, D. A., et al. 2009, A&A, 497, 729
Feulner, G., Gabasch, A., Salvato, M., et al. 2005, ApJ, 633, L9
Finkelstein, S. L., Hill, G. J., Gebhardt, K., et al. 2011, ApJ, 729, 140
Franceschini, A., Rodighiero, G., Cassata, P., et al. 2006, A&A, 453, 397
Fruchter, A. S., & Hook, R. N. 2002, PASP, 114, 144
Fynbo, J. P. U., Jakobsson, P., Möller, P., et al. 2003, A&A, 406, L63
Fynbo, J. P. U., Jakobsson, P., Prochaska, J. X., et al. 2009, ApJS, 185, 526
Fynbo, J. P. U., Möller, P., Thomsen, B., et al. 2002, A&A, 388, 425
Fynbo, J. P. U., Starling, R. L. C., Ledoux, C., et al. 2006, A&A, 451, L47
Hjorth, J., Møller, P., Gorosabel, J., et al. 2003, ApJ, 597, 699
Jakobsson, P., Björnsson, G., Fynbo, J. P. U., et al. 2005, MNRAS, 362, 245
Jensen, B. L., Fynbo, J. P. U., Hjorth, J., et al. 2005, GCN Circ., 3809, 1
Jones, T., Ellis, R., Jullo, E., & Richard, J. 2010, ApJ, 725, L176
Juneau, S., Glazebrook, K., Crampton, D., et al. 2005, ApJ, 619, L135
Kawai, N., Kosugi, G., Aoki, K., et al. 2006, Nature, 440, 184
Kewley, L. J., & Ellison, S. L. 2008, ApJ, 681, 1183
Kocevski, D., & West, A. A. 2011, ApJ, 735, L8
Köppen, J., Weidner, C., & Kroupa, P. 2007, MNRAS, 375, 673
Ledoux, C., Vreeswijk, P. M., Smette, A., et al. 2009, A&A, 506, 661
Leibler, C. N., & Berger, E. 2010, ApJ, 725, 1202
Levesque, E. M., Kewley, L. J., Berger, E., & Zahid, H. J. 2010a, AJ, 140, 1557
Levesque, E. M., Kewley, L. J., Graham, J. F., & Fruchter, A. S. 2010b, ApJ, 712, L26
Magdis, G. E., Rigopoulou, D., Huang, J., & Fazio, G. G. 2010, MNRAS, 401, 1521
Maiolino, R., Nagao, T., Grazian, A., et al. 2008, A&A, 488, 463
Makovoz, D., Roby, T., Khan, I., & Booth, H. 2006, Proc. SPIE, 6274, 62740C-1
Mannucci, F., Cresci, G., Maiolino, R., Marconi, A., & Gnerucci, A. 2010, MNRAS, 408, 2115
Mannucci, F., Cresci, G., Maiolino, R., et al. 2009, MNRAS, 398, 1915
Maraston, C. 2005, MNRAS, 362, 799
Marchesini, D., van Dokkum, P., Quadri, R., et al. 2007, ApJ, 656, 42
Ono, Y., Ouchi, M., Shimasaku, K., et al. 2010, MNRAS, 402, 1580
Peng, C. Y., Ho, L. C., Impey, C. D., & Rix, H. 2002, AJ, 124, 266
Perley, D. A., Cenko, S. B., Bloom, J. S., et al. 2009, AJ, 138, 1690
Price, P. A., Songaila, A., Cowie, L. L., et al. 2007, ApJ, 663, L57
Prochaska, J. X., Chen, H., Dessauges-Zavadsky, M., & Bloom, J. S. 2007, ApJ, 666, 267
Prochaska, J. X., Chen, H.-W., Wolfe, A. M., Dessauges-Zavadsky, M., & Bloom, J. S. 2008, ApJ, 672, 59
Prochaska, J. X., Sheffer, Y., Perley, D. A., et al. 2009, ApJ, 691, L27
Reddy, N. A., Steidel, C. C., Erb, D. K., Shapley, A. E., & Pettini, M. 2006, ApJ, 653, 1004
Rolleston, W. R. J., Smartt, S. J., Dufton, P. L., & Ryans, R. S. I. 2000, A&A, 363, 537
Salvaterra, R., Della Valle, M., Campana, S., et al. 2009, Nature, 461, 1258
Savaglio, S., Glazebrook, K., & Le Borgne, D. 2009, ApJ, 691, 182
Savaglio, S., Glazebrook, K., Le Borgne, D., et al. 2005, ApJ, 635, 260
Shapley, A. E., Steidel, C. C., Erb, D. K., et al. 2005, ApJ, 626, 698
Talbot, R. J., Jr., & Arnett, W. D. 1971, ApJ, 170, 409
Tanvir, N. R., Barnard, V. E., Blain, A. W., et al. 2004, MNRAS, 352, 1073
Tanvir, N. R., Fox, D. B., Levan, A. J., et al. 2009, Nature, 461, 1254
Thöne, C. C., Kann, D. A., Jóhannesson, G., et al. 2010, A&A, 523, A70
Totani, T., Kawai, N., Kosugi, G., et al. 2006, PASJ, 58, 485
Tremonti, C. A., Heckman, T. M., Kauffmann, G., et al. 2004, ApJ, 613, 898
van Zee, L., Salzer, J. J., Haynes, M. P., O'Donoghue, A. A., & Balonek, T. J. 1998, AJ, 116, 2805
Vila-Costas, M. B., & Edmunds, M. G. 1992, MNRAS, 259, 121
Vreeswijk, P. M., Ellison, S. L., Ledoux, C., et al. 2004, A&A, 419, 927
Woosley, S. E., & Bloom, J. S. 2006, ARA&A, 44, 507
Zahid, H. J., Kewley, L. J., & Bresolin, F. 2011, ApJ, 730, 137